Natural Resources Canada
Ressources naturelles Canada

Estimates of garnet crystallization and rates of metamorphism for metapelites of the Snowcap assemblage, Yukon-Tanana terrane, Yukon

Y.E. Morneau, F. Gaidies, J.J. Ryan, and A. Zagorevski

Geological Survey of Canada
Current Research 2017-2

2017

Geological Survey of Canada
Current Research 2017-2

Estimates of garnet crystallization and rates of metamorphism for metapelites of the Snowcap assemblage, Yukon-Tanana terrane, Yukon

Y.E. Morneau, F. Gaidies, J.J. Ryan, and A. Zagorevski

2017

ISSN 1701-4387
ISBN 978-0-660-09074-0
Catalogue No. M44-2017/2E-PDF
https://doi.org/10.4095/304229

A copy of this publication is also available for reference in depository libraries across Canada through access to the Depository Services Program's Web site at http://dsp-psd.pwgsc.gc.ca.

This publication is available for free download through GEOSCAN (http://geoscan.nrcan.gc.ca).

Recommended citation

Morneau, Y.E., Gaidies, F., Ryan, J.J., and Zagorevski, A., 2017. Estimates of garnet crystallization and rates of metamorphism for metapelites of the Snowcap assemblage, Yukon-Tanana terrane, Yukon; Geological Survey of Canada, Current Research 2017-2, 21 p. https://doi.org/10.4095/304229

Critical review

D. Regis

Authors

Y.E. Morneau (YannickMorneau@cmail.carleton.ca)
F. Gaidies (Fred_Gaidies@carleton.ca)
Department of Earth Sciences
2115 Herzberg Laboratories, Carleton University
1125 Colonel By Drive
Ottawa, Ontario
K1S 5B6

J.J. Ryan (Jim.Ryan@canada.ca)
Geological Survey of Canada
605 Robson Street
Vancouver, British Columbia
V6B 5J3

A. Zagorevski (Alex.Zagorevski@canada.ca)
Geological Survey of Canada
601 Booth Street
Ottawa, Ontario
K1A 0E8

Correction date:

Estimates of garnet crystallization and rates of metamorphism for metapelites of the Snowcap assemblage, Yukon-Tanana terrane, Yukon

Morneau, Y.E., Gaidies, F., Ryan, J.J., and Zagorevski, A., 2017. Estimates of garnet crystallization and rates of metamorphism for metapelites of the Snowcap assemblage, Yukon-Tanana terrane, Yukon; Geological Survey of Canada, Current Research 2017-2, 21 p. https://doi.org/10.4095/304229

Abstract: Amphibolite-facies Snowcap assemblage rocks in the Stewart River area (west-central Yukon) preserve significant information on the tectonometamorphic history of the Yukon-Tanana terrane. Garnet-bearing metapelites were analyzed to obtain detailed metamorphic pressure-temperature-time (P-T-t) information through the integration of whole-rock geochemistry, electron-microprobe analysis, X-ray micro–computed tomography, phase equilibria, and garnet-crystallization modelling. The bulk chemistry of the Snowcap assemblage rocks indicates that their protoliths are shale and wacke that were deposited in a passive-margin setting. Textural observations indicate at least three episodes of deformation, forming an early schistosity (S_{M-2}) overprinted by a crenulation cleavage (S_{M-1}) defined by quartz and ilmenite inclusions in garnet, and a dominant transposition foliation (S_M) mainly recorded by micaceous layers. Compositional zoning of garnet with respect to its Fe, Mg, Mn, Ca, and Y contents indicates chemical disequilibrium across the garnet volume and between garnet and the rock matrix. The zoning is interpreted to result from chemical fractionation associated with garnet growth and relatively slow intracrystalline diffusion. Calculations on a key sample indicate garnet started to crystallize at approximately 510°C and 3.75 kbar and finished growing at about 670°C and 6.8 kbar. These conditions correspond to the peak P-T conditions experienced by the rock. The chemical composition of the garnet core indicates significant modification of the initial garnet chemistry by intracrystalline diffusion at temperatures of 600°C or higher for at least 20 Ma. There are no current age constraints on the samples analyzed, but previous studies indicate Permian and Jurassic diachronic and/or episodic regional metamorphism.

Résumé : Les roches de l'assemblage de Snowcap du faciès des amphibolites, dans la région de la rivière Stewart (centre-ouest du Yukon), préservent de l'information importante sur l'histoire tectono-métamorphique du terrane de Yukon-Tanana. Nous avons analysé des métapélites à grenat pour obtenir des renseignements détaillés sur la pression, la température et la durée du métamorphisme, en intégrant la géochimie sur roche totale, l'analyse par microsonde électronique, la microtomographie à rayons X assistée par ordinateur, l'équilibre des phases et la modélisation de la cristallisation des grenats. La composition chimique des roches de l'assemblage de Snowcap indique que leurs protolites étaient des shales et des wackes déposés sur une marge passive. Nos observations texturales indiquent qu'il y a eu au moins trois épisodes de déformation, formant d'abord une schistosité (S_{M-2}) qui a été surimprimée par un clivage de crénulation (S_{M-1}) défini par des inclusions de quartz et d'ilménite dans les grenats, puis par une foliation de transposition dominante (S_M) principalement définie par des couches micacées. La zonation des grenats quant à leur teneur en Fe, Mg, Mn, Ca et Y indique un déséquilibre chimique à l'intérieur de chaque cristal, ainsi qu'entre les grenats et la matrice rocheuse. Selon notre interprétation, cette zonation résulte du fractionnement chimique associé à la croissance des grenats et à une diffusion intracristalline relativement lente. Nos calculs sur un échantillon clé indiquent que la cristallisation des grenats a commencé à environ 510 °C et 3,75 kbar et s'est terminée à environ 670 °C et 6,8 kbar. Ces conditions correspondent aux conditions maximales de pression et de température subies par la roche. La composition chimique du cœur de ce grenat indique une modification importante de la composition initiale des grenats par diffusion intracristalline à des températures d'au moins 600 °C, pendant 20 millions d'années ou plus. Il n'y a pas de paramètres contraignant l'âge des échantillons analysés, mais des études antérieures ont indiqué un métamorphisme régional diachronique et/ou épisodique au Permien et au Jurassique.

INTRODUCTION

The detailed study of metamorphic garnet crystallization and its effect on the thermodynamically effective bulk-rock composition is essential for the high-precision determination of the associated pressure-temperature-time (P-T-t) path. Cations of Fe, Mg, Ca, and Mn have significantly lower diffusion rates in garnet relative to other major metamorphic minerals (Chakraborty and Ganguly, 1992), resulting in chemical zoning in garnet and reflecting changes in the physicochemical environment during its growth (Carlson, 2006). Growth of garnet requires nutrients from the bulk-rock composition, and diffusion across individual garnet grains is too slow to establish chemical equilibrium with the rock matrix. Therefore, garnet growth causes incremental changes in the effective bulk-rock chemistry, resulting in fractional crystallization of garnet. The proportion of garnet end-members that crystallize at any incremental growth stage is pressure- and temperature- dependent, and reflects the effective bulk-rock composition that is available at the time. Generally, Fe and Mg contents of garnet in metapelites increase with increasing temperature during growth and are relatively weakly pressure-dependent (Ferry and Spear, 1978; Spear et al., 1991). The Ca content of garnet is more pressure-sensitive than that of the other major cations and generally increases with increasing pressure (e.g. Ghent 1975). Manganese commonly decreases from core to rim, since it is a minor chemical component in metapelitic rocks that is preferentially consumed by garnet and rapidly depleted in the bulk rock as garnet grows (Spear et al., 1991). Chemical diffusion in garnet can have an important effect on the zoning of these cations depending on temperature, time, and garnet crystal size. Diffusion in garnet becomes effective at T>585–600°C (Caddick et al., 2010; Florence and Spear, 1991) for times of 5 Ma or longer, and has a more significant influence on Mn and Fe compared to its other major cations.

In this study, we reconstruct the metamorphic P-T-t path associated with garnet crystallization in metapelitic rocks of the Snowcap assemblage of the Yukon-Tanana terrane exposed in the Stewart River area (Fig. 1). This area has previously been a focus of regional geological mapping and regional metamorphic studies (Gordey and Ryan, 2005; Berman et al., 2007; Staples et al., 2014; 2016). Herein, we present new petrographic and geochemical data on the Yukon-Tanana terrane garnet-mica schists and utilize their mineral assemblages, bulk-rock and garnet chemical compositions, and rock textures to infer the conditions of their metamorphism. Garnet-crystallization simulations accounting for garnet fractionation and intracrystalline diffusion are used to constrain the P-T-t path. We demonstrate that the consideration of garnet fractionation during metamorphism results in significantly different and better constrained P-T-t–path estimates compared to the commonly used phase-equilibrium approach, where the thermodynamically effective chemical composition of the rock is assumed to be fixed during metamorphism.

REGIONAL GEOLOGY

The northern Cordilleran orogen formed by successive accretion of allochthonous terranes to the western Laurentian margin, thought to have started in the Late Permian (Beranek and Mortensen, 2011) and continued throughout the Mesozoic (Monger and Price, 2002; Nelson et al., 2013; Staples et al., 2016). Collectively referred to as the peri-Laurentian terranes, these terranes include intra-oceanic arcs (Quesnel and Stikine terranes), arcs built on continental fragments (Yukon-Tanana terrane), and remnants of an ocean basin (Slide Mountain terrane) that separated arc terranes from the Laurentian margin. Orogenic events associated with intra-oceanic deformation and accretion of terranes generated widespread amphibolite-facies metamorphism throughout the Yukon-Tanana terrane and the Laurentian margin at different times (Berman et al., 2007). Quantitative studies of the regional metamorphism have been conducted at both local and broadly regional scales (Dusel-Bacon et al., 1995; Berman et al., 2007; Staples et al., 2013, 2014; Clark et al., 2016), but are too sparse to provide a coherent regional framework. These studies do however indicate that amphibolite-facies metamorphism was episodic and/or diachronic, with documented events occurring in the Permo-Triassic, Early Jurassic, Middle to Late Jurassic, and Early to mid-Cretaceous (Staples et al., 2016).

Deposition of sediments on the western Laurentian margin began during the Neoproterozoic rifting of Rodinia (Dickinson, 2004; Nelson et al., 2013) and continued into the Late Devonian. These sediments became the basement to the Paleozoic arcs of the Yukon-Tanana terrane (Nelson et al., 2013 and references therein). In most models, the Yukon-Tanana terrane is considered to have separated from the Laurentian margin by back-arc rifting of a Devono-Mississippian arc and the development of the Slide Mountain ocean basin, and experienced several phases of arc magmatism and tectonism prior to its re-accretion to the Laurentian margin in the Late Permian to Early Triassic (Beranek et al., 2010) or Jurassic (e.g. Berman et al., 2007). Subsequent to this, the Yukon-Tanana terrane became the basement to Mesozoic magmatism, which resulted in emplacement of rare Triassic and voluminous Jurassic to Cretaceous plutons (Woodsworth et al., 1991; Logan and Mihalynuk, 2014).

Yukon-Tanana terrane

The Yukon-Tanana terrane is a composite terrane that went through several phases of deformation and medium- to high-grade metamorphism (Berman et al., 2007; Staples et al., 2016). It consists of four regional tectonostratigraphic assemblages (Fig. 1): a basal siliciclastic assemblage of continental-margin affinity (Snowcap assemblage), overlain by three unconformity-bounded, mid- to late-Paleozoic volcano-sedimentary successions of continental-arc and back-arc affinities (Finlayson, Klinkit, and Klondike assemblages) (Piercey et al., 2006). The Snowcap assemblage

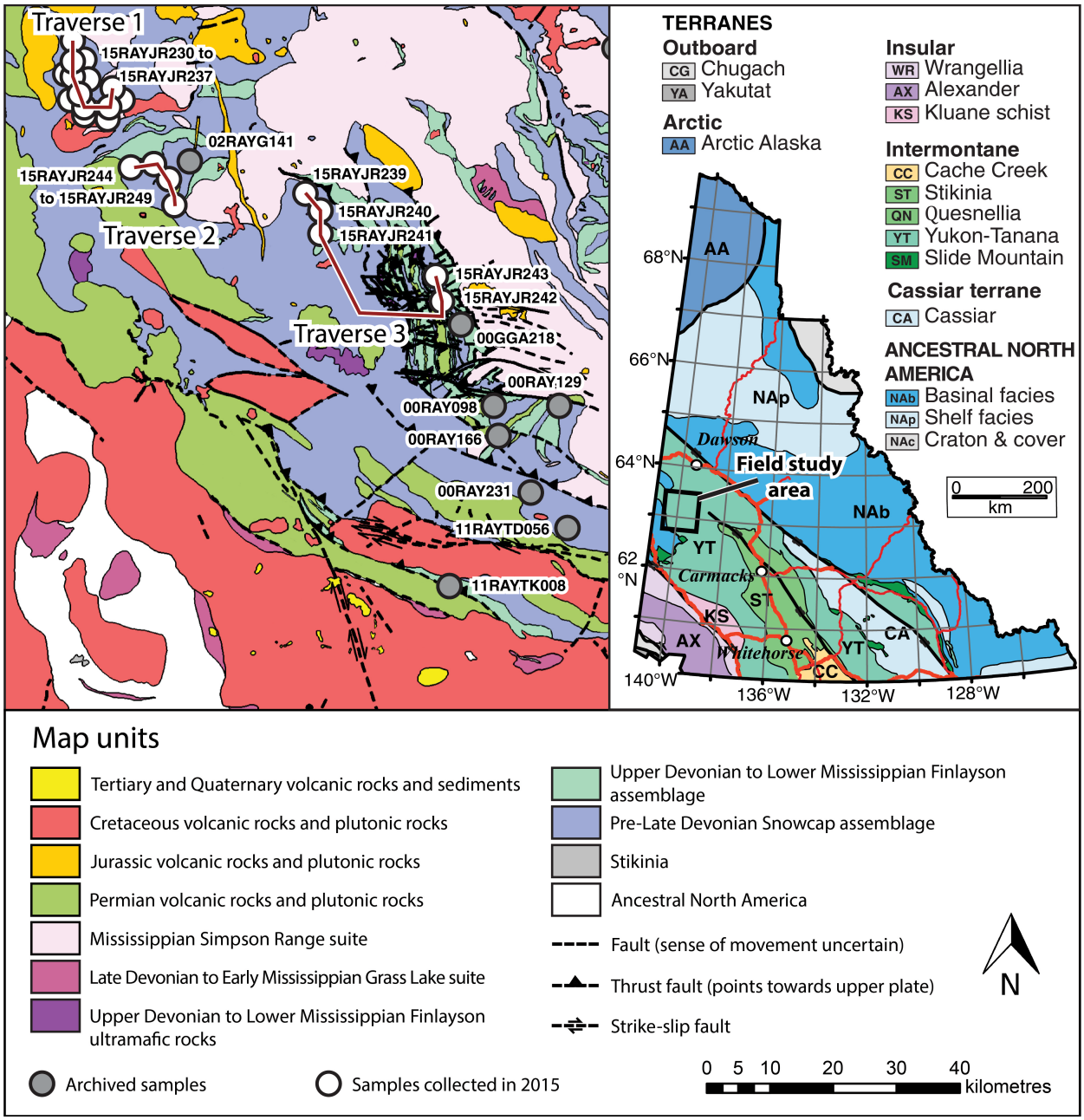

Figure 1. Regional field-area map in the Stewart River area. The locations of sample collection and traverses done during the 2015 field season are shown. Figure *modified from* Yukon Geological Survey, 2016, Yukon Digital Bedrock Geology (sourced from Gordey and Ryan, 2005; Ryan et al., 2014). Terrane map *modified from* Colpron and Nelson (2011).

constitutes the oldest unit of the Yukon-Tanana terrane and is characterized by pre-Late Devonian metasedimentary rocks and amphibolite (Piercey and Colpron, 2009). It is overlain by the Carboniferous Finlayson, Lower Permian Klinkit, and Permian Klondike assemblage volcanic rocks and intruded by the Early Mississippian Simpson Range and the Middle Permian Sulphur Creek suite. In west-central Yukon, units of the Yukon-Tanana terrane are intruded by the widespread early Jurassic Minto and Long Lake plutonic suites and the mid-Cretaceous Whitehorse plutonic suite (dominated by the Dawson Range phase) (Joyce et al., 2015; Berman et al., 2007; Colpron and Ryan, 2009; Ryan et al., 2014).

In the Stewart River area, the Yukon-Tanana terrane was subjected to three major episodes of metamorphism (Berman et al., 2007; Staples et al., 2014). The first, low-pressure metamorphic episode is indicated by growth of metamorphic sphene at 365–350 Ma (Berman et al., 2007). This episode may represent contact metamorphism associated with the emplacement of the Mississippian Simpson

Range suite plutons and/or a cryptic episode of regional deformation (Berman et al., 2007). A second, medium-pressure metamorphic event occurred between 260 and 240 Ma, reaching peak metamorphic conditions of 9 kbar and 600°C. The cause of this metamorphism is contentious. Berman et al. (2007) interpreted this metamorphic episode to be related to intra-arc thickening of the Yukon-Tanana terrane during the closure of the Slide Mountain Ocean, and not to a collision with North America, based on the lack of any known deformation or metamorphism in North American rocks. Beranek and Mortensen (2011) interpreted the same episode to be associated with the terminal closure of the Slide Mountain basin and collision of the Yukon-Tanana terrane with the North American margin, based on the presence of Permian detritus in the Triassic sedimentary assemblage overlap on the North American margin that were most likely derived from the Yukon-Tanana terrane. In contrast, Canil et al. (2003) and Johnston et al. (2007) identified an exhumed peridotite massif within the Yukon-Tanana terrane, indicating a major Middle Permian extensional episode.

The third metamorphic event in the Yukon-Tanana terrane occurred during the Jurassic, between 195 and 187 Ma, reaching peak P-T conditions of about 7.8 kbar and 595°C (Berman et al., 2007; Staples et al., 2014). Significant crustal reworking in the Late Jurassic and Cretaceous culminated in the exhumation of deep metamorphic rocks in mid-Cretaceous core complexes (Staples et al., 2013, 2016). These core complexes expose rocks of the parautochthonous Laurentia, similar in age and composition to the siliciclastic foundation of the Yukon-Tanana terrane, but lacking the Mississippian to Permian history of that terrane. The extent of the various phases of metamorphism is generally poorly constrained regionally, as only a few modern metamorphic and geochronological studies have been conducted on relatively rare high-variance metamorphic assemblages (Berman et al., 2007; Staples et al., 2013; Clark et al., 2016). These studies assumed bulk-rock equilibrium and did not utilize garnet-crystallization modelling. Additionally, there are few locations with rocks of appropriate bulk chemical composition and mineral content required to best constrain the metamorphic conditions experienced. Rocks best suited for high-precision metamorphic P-T-t path identification include metapelites ranging from greenschist to upper-amphibolite facies.

Snowcap assemblage

The Snowcap assemblage comprises mostly pre-late Devonian deformed and metamorphosed siliciclastic rocks, including quartzite, micaceous quartzite, psammitic schist, carbonaceous schist, marble, calc-silicate rocks, amphibolite, and garnet amphibolite (Colpron and Ryan, 2009; Piercey and Colpron, 2009; Ryan et al., 2014). These rocks commonly preserve evidence of polyphase deformation and metamorphism, including syn- and post-tectonic mineral growth (Berman et al. 2007; Piercey and Colpron, 2009).

Metapelitic and metapsammitic rocks are commonly interlayered with quartzite and are intruded by felsic dykes and sills. These include the Mississippian Simpson Range suite, the Permian Sulphur Creek suite, and the Jurassic Minto and Long Lakes suites. The main schistosity in the metapelitic rocks is generally shallowly dipping with variable strike orientations. Snowcap assemblage metapelitic rocks with good index minerals such as garnet, kyanite, and staurolite are not widespread in the Stewart River area, and therefore outcrops known to contain garnet from previous work (Gordey et al., 2006) were targeted. For the purpose of this study, newly collected and archived (Gordey and Ryan, 2005) metapelitic to metapsammitic garnet-bearing samples of the Snowcap assemblage were selected (Fig. 1, Table 1). All samples were subjected to whole-rock chemical analysis. Samples 00RAY098A, 00RAY231A, 15RAYJR237B, and 15RAYJR246A were used as representative samples for sample description and thermodynamic phase-equilibrium modelling. Samples 15RAYJR232A and 15RAYJR244A were used for textural analyses. Sample 15RAYJR246A was used for X-ray micro–computed tomography, electron-microprobe analysis, and garnet-crystallization modelling, as its mineralogy and whole-rock chemistry are most representative of all samples.

METHODS

X-ray fluorescence (XRF) and inductively coupled plasma optical-emission spectrometry (ICP-OES)

For each sample under investigation, an average volume of about 200 cm^3 of material was sent for lithogeochemical analysis at Activation Laboratories (Ancaster, Ontario). The analytical results are given in Table 2. Samples were pulverized using an agate mill. Major-element concentrations were determined using X-ray fluorescence (XRF) analysis. Loss on ignition was measured prior to fusion by heating the samples at 1000°C for 2 hours. About 0.75 g of the remaining homogenized sample was fused with 9.75 g of lithium metaborate and lithium tetraborate in Pt crucibles, and then poured into Pt moulds. Lithium bromide was used as a releasing agent. The major-element concentrations were then measured using a Panalytical Axios Advanced wavelength-dispersive XRF instrument. The detection limit was approximately 0.01 weight % for most elements, using the method of Norrish and Hutton (1969).

Trace concentrations of Zr were measured using inductively coupled plasma optical-emission spectrometry (ICP-OES). Samples were mixed with lithium metaborate and lithium tetraborate, melted in an induction furnace and allowed to cool, then mixed with 5% nitric acid until completely dissolved. Some trace elements and oxides were then measured using a Varian Vista 735 ICP instrument.

Table 1. Sample locations (NAD83).

Sample ID	Latitude	Longitude	Sample ID	Latitude	Longitude
00GGA218A	63.126	-139.318	**15RAYJR231A**	63.432	-140.332
00RAY098A	63.025	-139.229	**15RAYJR232A**	63.429	-140.333
00RAY129A	63.022	-139.054	**15RAYJR232A**	63.429	-140.333
00RAY166A	62.988	-139.223	**15RAYJR233A**	63.423	-140.328
00RAY226B	63.760	-138.514	**15RAYJR235A**	63.406	-140.325
00RAY231A	62.920	-139.140	**15RAYJR236B**	63.398	-140.296
02RAY080A	63.413	-140.325	**15RAYJR237B**	63.408	-140.278
02RAYG039C	63.328	-140.133	**15RAYJR239A**	63.278	-139.712
02RAYG141A	63.361	-140.057	**15RAYJR240A**	63.269	-139.704
02RAYG158A	63.412	-140.024	**15RAYJR241A**	63.253	-139.696
03GGA451A	63.585	-139.029	**15RAYJR242A**	63.161	-139.369
03GGAR040A	63.461	-138.875	**15RAYJR242B**	63.161	-139.369
10RAYJR049A	62.646	-137.922	**15RAYJR243A**	63.186	-139.384
11RAYAZ421	62.694	-137.890	**15RAYJR244A**	63.330	-140.163
11RAYJR070A	62.991	-138.414	**15RAYJR245A**	63.329	-140.154
11RAYTD056A	62.873	-139.042	**15RAYJR246A**	63.327	-140.133
11RAYTK008	62.805	-139.362	**15RAYJR248A**	63.325	-140.121
15RAYJR230A	63.438	-140.334	**15RAYJR249A**	63.316	-140.108

The detection limit was 0.01 weight % for most oxides, 0.001 weight % for MnO and TiO_2, and 1 to 5 ppm for trace elements.

X-ray micro - computed tomography (XR-µCT)

A 27 cm^3 block of sample 15RAYJR246A was scanned using a SkyScan 1173 instrument at Carleton University (Ottawa, Ontario) with a 130 kV and 61 µA X-ray source and a brass filter in order to obtain its garnet crystal-size distribution. The block was scanned for 180° using 0.3° step sizes. The largest garnet crystal was identified and processed to obtain a cross-section through its geometric core. The section was used to analyze the compositional zoning of garnet. Comparison of the section with the XR-µCT data set indicates a maximum deviation from the geometric core of garnet of about 30 µm.

Electron-microprobe analysis

An electron-microprobe transect was analyzed across the centre of the largest garnet crystal in sample 15RAYJR246A using a Cameca Camebax MBX electron probe micro analyzer at Carleton University. Analyses were done using an accelerating potential of 20 kV and a beam current of 20.7 nA. Peak counting times were either 62 500 counts or 30 seconds. The Cameca PAP matrix-correction software was used to convert counts into weight per cent. Eighty-seven analyses were done for the transect, resulting in a spacing of approximately 35 µm.

Thermodynamic phase equilibria and garnet-crystallization modelling

Pressure-temperature phase-equilibrium diagrams were constructed using the DOMINO software (de Capitani and Petrakakis, 2010). The bulk-rock chemistry of samples 00RAY231A, 00RAY098A, 15RAYJR237B, and 15RAYJR246A (Table 2) was used to determine the stable mineral assemblages and garnet compositions across projected P-T fields within the $MnO\text{-}Na_2O\text{-}CaO\text{-}K_2O\text{-}FeO\text{-}MgO\text{-}Al_2O_3\text{-}SiO_2\text{-}H_2O\text{-}TiO_2$ model system. The Fe_2O_3 species was not included in the system due to the absence of magnetite, and of ferric iron in ilmenite and garnet. The thermodynamic database of Holland and Powell (1998) was used for the modelling. For details about the activity models used in our calculations, the reader is referred to Gaidies et al. (2015). A metamorphic P-T-t path was calculated based on garnet-crystallization modelling using the THERIA_G software (Gaidies et al., 2008) and the same thermodynamic data set used for the phase-equilibrium modelling. The P-T-t path was compared to the phase-equilibrium diagram of the fractionated chemistry of the rock, which was extracted from the THERIA_G model results. The kinetic data set of Chakraborty and Ganguly (1992) was used for intracrystalline-diffusion simulations.

Table 2. Whole-rock chemistry of all samples. For the 'Protolith' column, if (100 TiO_2/Zr)≥0.4, the protolith is a pelite, and if (100 TiO_2/Zr)<0.4, the protolith is a psammite (Psam) (Garcia et al., 1991). Pale grey rows indicate samples which were used for phase-equilibrium modelling. The darker grey row corresponds to the sample that was used for garnet-crystallization modelling.

	NiO	SiO_2	Al_2O_3	Fe_2O_3	MnO	MgO	CaO	Na_2O	K_2O	TiO_2	P_2O_5	Cr_2O_3	LOI	Total	Zr	100 TiO_2/Zr	Protolith
	(weight %)														(ppm)		
Analysis	XRF	XRF	XRF	XRF	XRF	XRF	XRF	XRF	XRF	XRF	XRF	XRF	XRF	XRF	ICP	-	-
Detection limit	0.003	0.01	0.01	0.01	0.001	0.01	0.01	0.01	0.01	0.01	0.01	0.01		0.01	2	-	-
00GGA218A	0.006	66.58	13.19	5.87	0.087	2.96	3.22	1.02	2.74	0.69	0.11	0.01	4.46	101.00	264	0.26	Psam
00RAY098A	0.015	56.04	20.12	7.73	0.044	3.26	1.22	0.76	5.74	0.64	0.12	0.03	3.87	99.59	135	0.47	Pelite
00RAY129A	0.006	74.69	11.98	4.04	0.062	0.88	2.27	1.83	2.13	0.23	0.03	< 0.01	1.50	99.67	150	0.15	Psam
00RAY166A	0.004	64.20	17.09	5.58	0.084	1.68	2.24	1.98	3.70	0.71	0.11	0.01	2.01	99.41	290	0.24	Psam
00RAY231A	0.015	61.87	17.04	8.31	0.344	2.84	0.81	0.96	4.39	0.94	0.07	0.01	2.48	100.10	174	0.54	Pelite
02RAY080A	0.007	65.19	16.40	6.36	0.049	1.91	0.43	0.52	3.43	0.85	0.16	0.02	3.56	98.92	235	0.36	Psam
02RAYG039C	0.005	68.89	15.06	6.40	0.120	1.68	0.55	0.56	3.47	0.72	0.10	0.01	2.23	99.80	148	0.49	Pelite
02RAYG141A	0.004	57.09	22.63	7.04	0.080	1.80	0.33	0.63	5.31	0.93	0.16	0.02	3.58	99.63	215	0.43	Pelite
03GGA451A	0.004	64.46	14.06	8.29	0.255	1.98	0.77	0.59	4.14	0.80	0.21	0.01	3.22	98.83	157	0.51	Pelite
03GGAR040A	0.010	60.19	19.58	7.52	0.195	2.51	0.51	0.90	5.33	0.88	0.08	0.02	2.57	100.30	224	0.39	Psam
10RAYJR049A	0.009	58.93	18.09	9.31	0.102	2.84	1.29	1.33	3.70	1.22	0.11	0.01	2.62	99.60	251	0.49	Pelite
11RAYAZ421	0.004	56.26	20.52	10.03	0.101	2.51	0.87	1.16	3.95	1.47	0.09	0.01	3.22	100.20	359	0.41	Pelite
11RAYTD056A	0.003	57.67	19.81	9.88	0.118	3.10	0.88	1.09	3.10	1.41	0.09	0.01	3.34	100.50	235	0.60	Pelite
11RAYTK008	< 0.003	73.21	13.44	4.97	0.098	1.39	0.47	0.47	3.44	0.66	0.09	0.01	2.01	100.30	307	0.21	Psam
15RAYJR230A	< 0.003	66.21	16.90	5.33	0.018	1.52	0.26	0.53	4.01	0.83	0.13	0.01	2.99	98.76	272	0.31	Psam
15RAYJR231A	0.006	56.86	21.14	8.71	0.071	2.33	0.72	0.49	5.26	0.95	0.16	0.01	3.46	100.20	202	0.47	Pelite
15RAYJR232A	0.008	63.36	17.70	7.78	0.062	2.04	0.70	0.71	4.44	0.86	0.07	0.01	2.35	100.10	158	0.54	Pelite
15RAYJR232A	< 0.003	65.48	15.23	7.62	0.094	1.67	2.78	2.08	2.52	0.70	0.25	< 0.01	1.38	99.81	161	0.43	Pelite
15RAYJR233A	0.005	65.77	15.89	6.32	0.296	2.43	0.50	1.01	4.24	0.65	0.12	0.01	2.27	99.53	154	0.42	Pelite
15RAYJR235A	0.007	64.17	18.41	6.73	0.037	2.00	0.34	0.49	4.60	0.80	0.09	0.01	3.08	100.80	152	0.53	Pelite
15RAYJR236B	0.017	68.19	13.79	5.91	0.060	3.63	1.19	0.85	2.76	0.57	0.26	0.03	2.21	99.48	156	0.37	Psam
15RAYJR236B	0.016	74.78	11.84	4.82	0.062	1.65	0.81	0.30	2.74	0.64	0.08	0.03	1.90	99.68	118	0.54	Pelite
15RAYJR237B	0.014	69.90	14.28	5.81	0.036	1.89	0.47	0.44	3.02	0.78	0.14	0.03	2.71	99.53	236	0.33	Psam
15RAYJR239A	0.009	56.52	22.61	8.74	0.206	2.35	0.11	0.68	5.12	0.90	0.06	0.02	3.48	100.80	157	0.57	Pelite
15RAYJR240A	0.022	70.20	12.74	5.08	0.014	2.47	2.22	0.94	2.52	0.62	0.12	0.04	2.86	99.87	125	0.50	Pelite
15RAYJR241A	0.023	54.82	19.18	9.91	0.332	3.45	1.32	1.42	5.64	1.39	0.26	0.03	2.04	99.85	259	0.54	Pelite
15RAYJR242A	0.012	53.82	20.12	10.38	0.281	2.52	0.34	0.51	6.69	1.09	0.06	0.02	2.81	98.69	199	0.55	Pelite
15RAYJR242B	0.010	71.42	12.59	6.38	0.148	1.58	0.83	1.22	3.80	0.65	0.05	0.01	1.26	99.97	105	0.62	Pelite
15RAYJR243A	0.003	71.07	13.59	6.59	0.102	1.69	0.19	0.32	3.93	0.74	0.05	0.01	1.73	100.00	344	0.22	Psam
15RAYJR244A	0.011	68.72	15.01	6.15	0.090	1.97	0.94	0.48	3.79	0.67	0.08	0.02	2.22	100.20	248	0.27	Psam
15RAYJR244A	0.007	63.94	18.63	6.35	0.070	1.74	0.77	0.48	5.22	0.71	0.14	0.02	2.57	100.70	97	0.73	Pelite
15RAYJR245A	0.026	62.45	17.17	7.87	0.189	2.62	0.98	0.75	4.51	0.90	0.09	0.04	2.17	99.79	170	0.53	Pelite
15RAYJR246A	0.007	54.72	21.70	9.19	0.100	2.43	1.08	0.65	5.67	0.89	0.14	0.01	3.22	99.83	116	0.77	Pelite
15RAYJR248A	0.010	62.42	17.29	7.56	0.074	2.26	1.29	0.85	4.81	0.72	0.12	0.02	2.14	99.58	130	0.55	Pelite
15RAYJR249A	0.010	73.28	14.06	3.97	0.051	1.37	0.72	1.00	3.87	0.58	0.08	0.01	1.93	101.00	297	0.20	Psam

RESULTS

Sample description

Most schist samples contain the assemblage garnet+white mica+quartz+biotite±ilmenite±plagioclase (Fig. 2). Sample 00RAY098A additionally contains several apatite porphyroblasts. Sample 15RAYJR237B contains both prograde and retrograde chlorite, which are differentiated by their texture relative to the rock foliation and by their composition. Biotite is pseudomorphed by retrograde chlorite. Sample 15RAYJR246A contains rutile crystals that have ilmenite rims. Garnet in all samples forms anhedral to subhedral porphyroblasts between 0.1 and 8 mm in diameter that are wrapped by the mica foliation in the matrix. Inclusions in garnet consist mostly of ilmenite, quartz, and apatite. Scarce zircon, allanite, and monazite inclusions up to 5 µm in size are present. Inclusion-trail patterns and abundances vary by locality. Samples collected in the northwestern section of the field area (samples 15RAYJR232A, 15RAYJR237B, 15RAYJR244A, and 15RAYJR246A) contain garnet porphyroblasts with abundant quartz inclusions, which can form complex inclusion trails (Fig. 2c, d, e, f). Garnet porphyroblasts in samples collected in the eastern section of the field area (samples 00RAY098A and 00RAY231A) are scarce in quartz inclusions but contain randomly oriented ilmenite inclusions (Fig. 2a, b). Garnet crystals in sample 00RAY231A preserve core and rim phases that are clearly separated by a textural boundary (Fig. 2b). Chlorite occurs in these samples as a retrograde mineral and is commonly observed as rims on garnet, or replacing biotite. Quartz has a modal abundance of 20 to 50%, depending on the sample.

Samples 15RAYJR232A and 15RAYJR244A display up to three generations of structures. The main foliation (S_M) consists of a mica schistosity observed in all samples. This foliation wraps around garnet porphyroblasts. Quartz and ilmenite inclusion trails are observed within the porphyroblasts (Fig. 2) and exhibit a complex pre-S_M structural history, consisting of a previous foliation (S_{M-2}) and crenulation cleavage (S_{M-1}). Both S_{M-1} and S_{M-2} are oriented in a consistent direction across all garnet grains (Fig. 3), indicating that garnet was not rotating during its crystal growth. Garnet is syn- to post-tectonic with respect to S_{M-1}. The formation of S_M started near the end of garnet growth and is captured by inclusions subparallel to S_M in the outer rim of a few garnet crystals (e.g. Figure 2e). Only samples from the western section of the field area appear to contain S_{M-2}, and only a few samples within this area contain S_{M-1}.

Bulk-rock chemistry

The TiO_2 and Zr contents (Table 2) as well as log (Fe_2O_3/K_2O) over log (SiO_2/Al_2O_3) values indicate shale and wacke protoliths (Fig. 4). The TiO_2/Zr ratio discriminates between protoliths of pelitic versus psammitic composition (Garcia et al., 1991), with approximately 70% of the samples being of pelitic origin and the remainder being of psammitic origin. According to the Herron (1988) classification of sediments, the samples have shale to wacke protoliths (Fig. 4). Using the classification of Roser and Korsch (1986), the K_2O/Na_2O over SiO_2 ratio suggests a passive-margin depositional environment (Fig. 5). The K_2O/Al_2O_3 ratio ranges between 0.19 and 0.33, indicating that the samples reflect clay-rich rather than feldspathic protoliths (Cox et al., 1995). Samples plot on a trend with constant FeO and MgO ratios, but with varying $Al_2O_3 - 3K_2O$ contents (Fig. 6). The samples plot closer to the FeO apex of the AFM projection relative to the average metapelite of Symmes and Ferry (1991), but plot in a similar compositional space as the Snowcap assemblage metapelite and metapsammite samples analyzed by Piercey and Colpron (2009).

X-ray micro - computed tomography (XR-µCT)

Garnet crystal sizes in sample 15RAYJR246A have a normal, unimodal distribution (Fig. 7). A total of 482 garnet crystals were identified in a volume of 27 cm^3, or approximately 18.7 garnet crystals per cm^3. The majority of crystals range between 0.9 and 2 mm in diameter, with the largest crystal having a diameter of 3 mm. The larger crystals are the least abundant.

Garnet compositional zoning

The largest garnet crystal in sample 15RAYJR246A is compositionally zoned from core to rim (Fig. 8, 9; Table 3). Zoning is symmetrical, with the core of the garnet crystal starting at 1.5 mm from the edge of the rim on each side. The mole fraction of iron (X_{Fe} = Fe/(Fe + Mg + Ca + Mn)) increases from 0.59 at the core to 0.72 near the rim; it does not change significantly for the outermost 0.4 mm of garnet near the rim. The mole fraction of Mg (X_{Mg}) increases from 0.035 at the core to 0.07 at a distance of 0.2 mm from the rim, and sharply increases to 0.13 toward the rim. The mole fraction of Ca (X_{Ca}) increases slightly for the first 0.8 mm away from the core, from 0.21 to 0.24, and then decreases sharply toward the rim to 0.15. The mole fraction of Mn (X_{Mn}) decreases continuously from core to rim, from 0.16 to 0.01.

Metamorphic phase equilibria

Phase-equilibrium diagrams calculated for samples 00RAY098A, 00RAY231A, 15RAYJR237B, and 15RAYJR246A on the basis of their bulk chemistry (Table 2) are shown in Figure 10. The P-T fields of garnet-bearing assemblages (light grey in Fig. 10) differ, reflecting differences in bulk chemistry between the samples. The diagrams clearly demonstrate the effect of bulk MnO content on the stability of garnet-bearing assemblages. Higher MnO concentration favours crystallization of garnet at significantly lower P-T

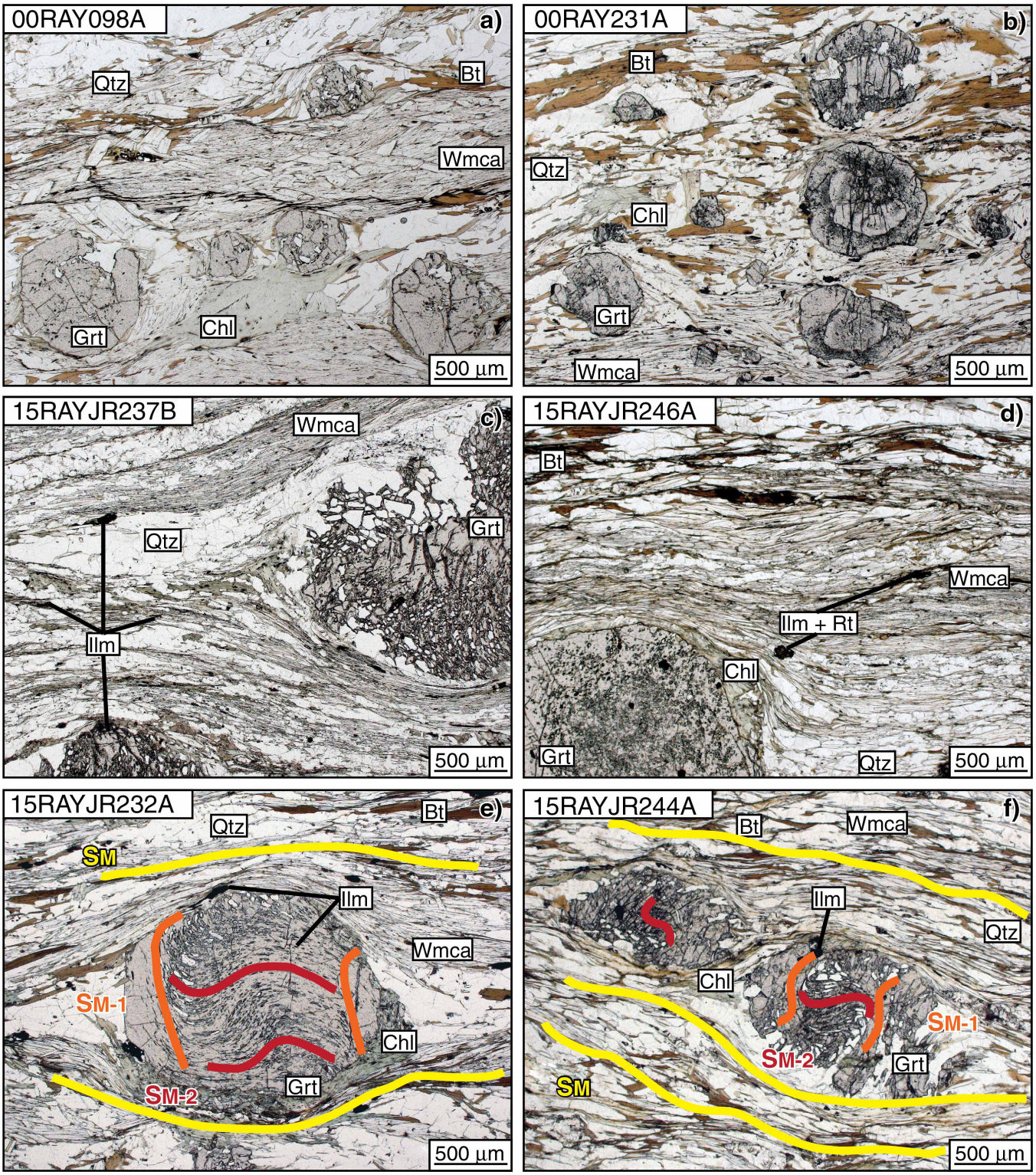

Figure 2. Microphotographs (plane-polarized light) illustrating the mineral assemblages and microstructures of representative samples. Figures 2e and 2f show garnet crystals containing inclusion trails with possible relict crenulation cleavage. Wmca = white mica. Other mineral abbreviations *from* Siivola and Schmid (2007).

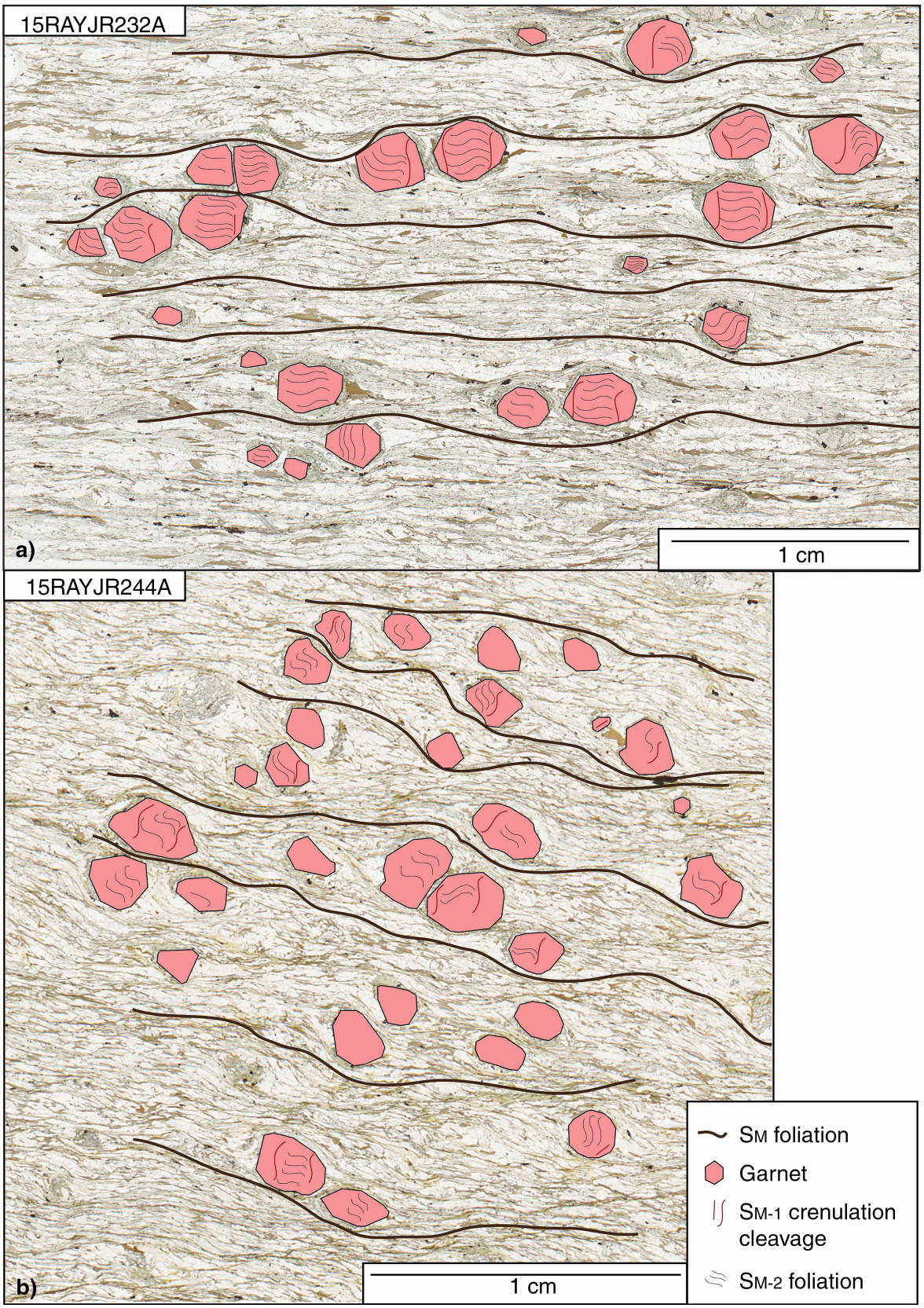

Figure 3. Sketches of microstructures across the thin sections for samples **a)** 15RAYJR232A and **b)** 15RAYJR244A.

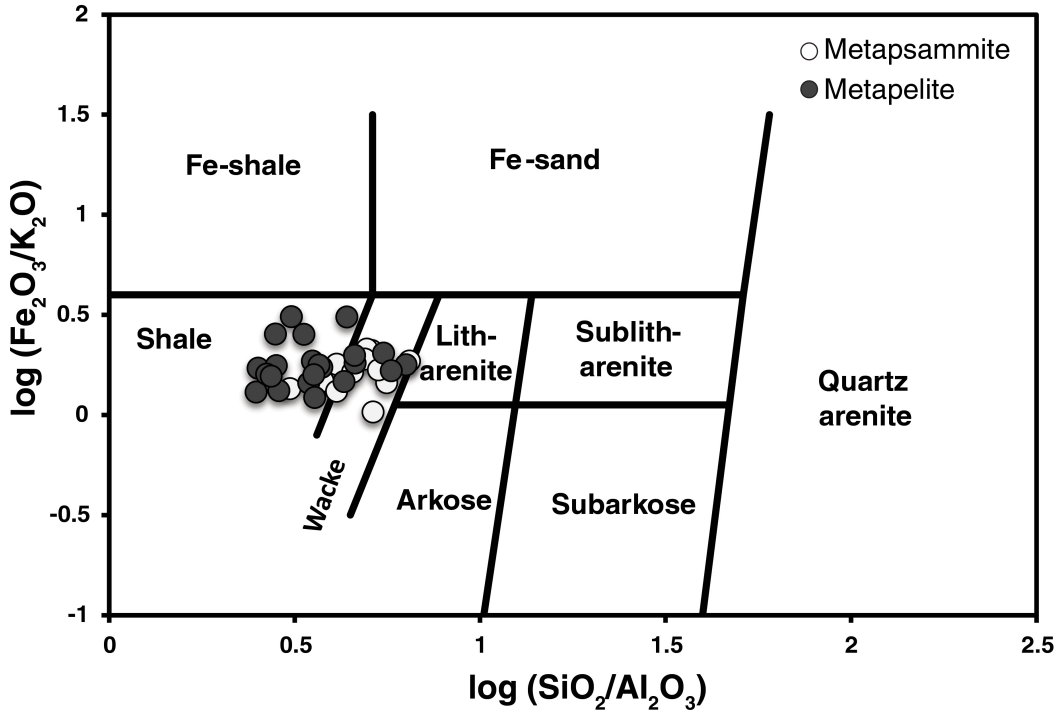

Figure 4. Sedimentary protoliths of samples (*modified from* Herron, 1988). The distinction between metapelite and metapsammite comes from the 100 TiO_2/Zr ratio (Table 2; Garcia et al., 1991).

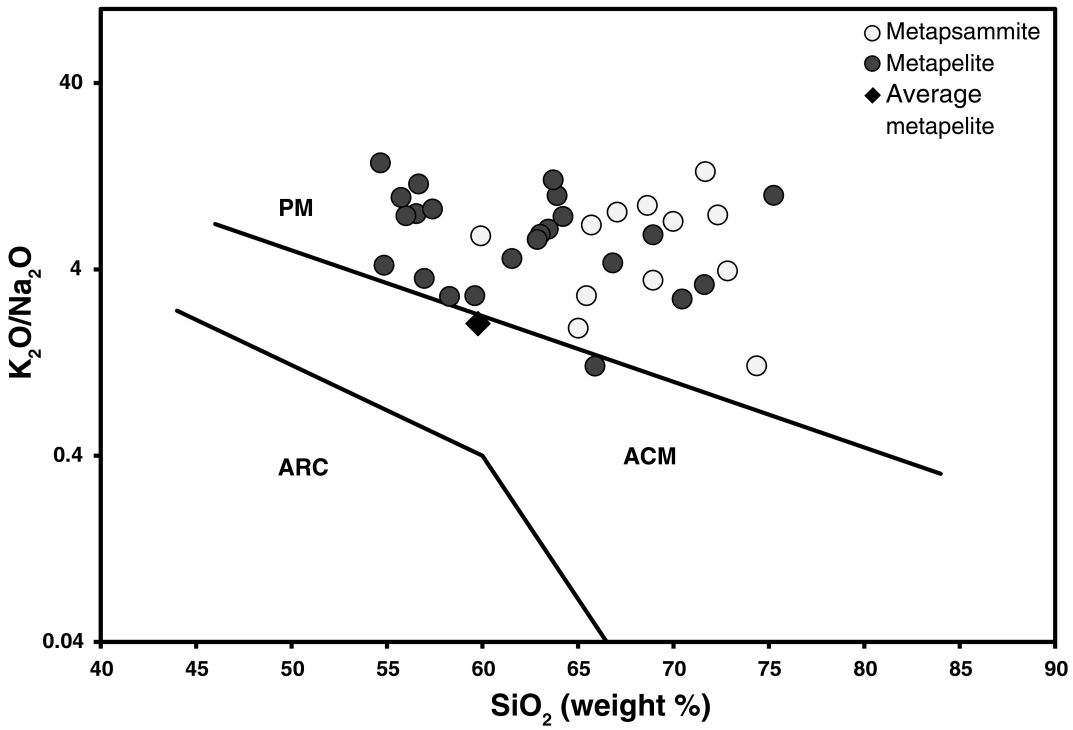

Figure 5. Depositional settings of protoliths (*modified from* Roser and Korsch, 1986). PM = passive margin; ACM = active continental margin; ARC = oceanic island arc. Average pelite composition according to Symmes and Ferry (1991).

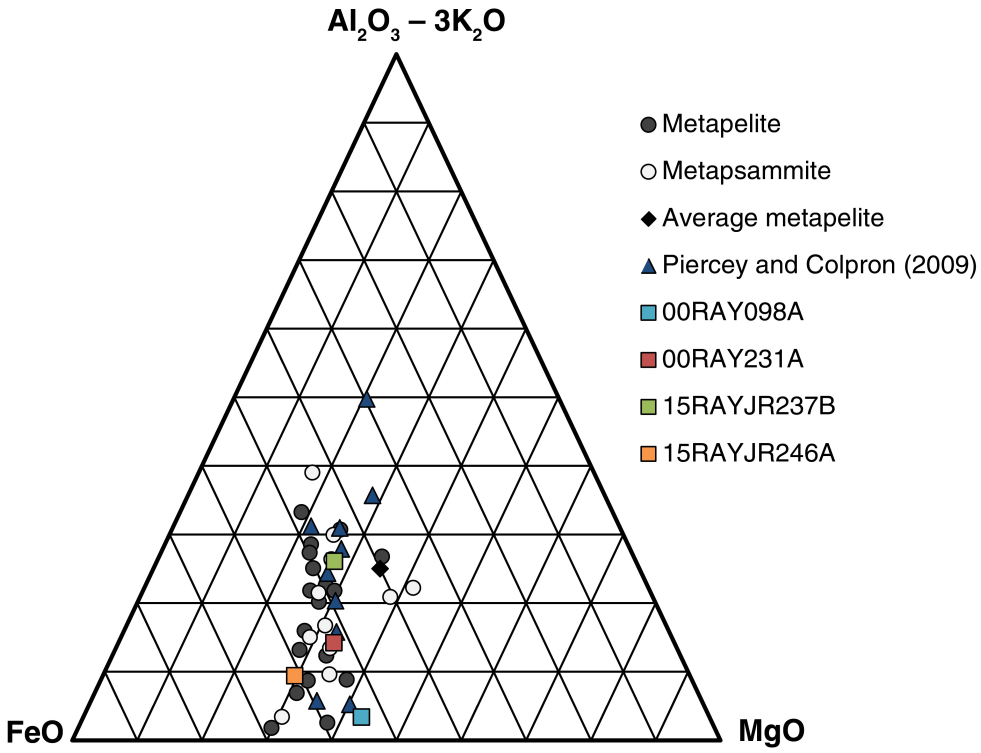

Figure 6. AFM projection from muscovite, quartz, and H_2O (*from* Thompson, 1957) of bulk-rock chemistry of all the samples collected. Total iron is assumed to be FeO. The average metapelite composition is that of Symmes and Ferry (1991).

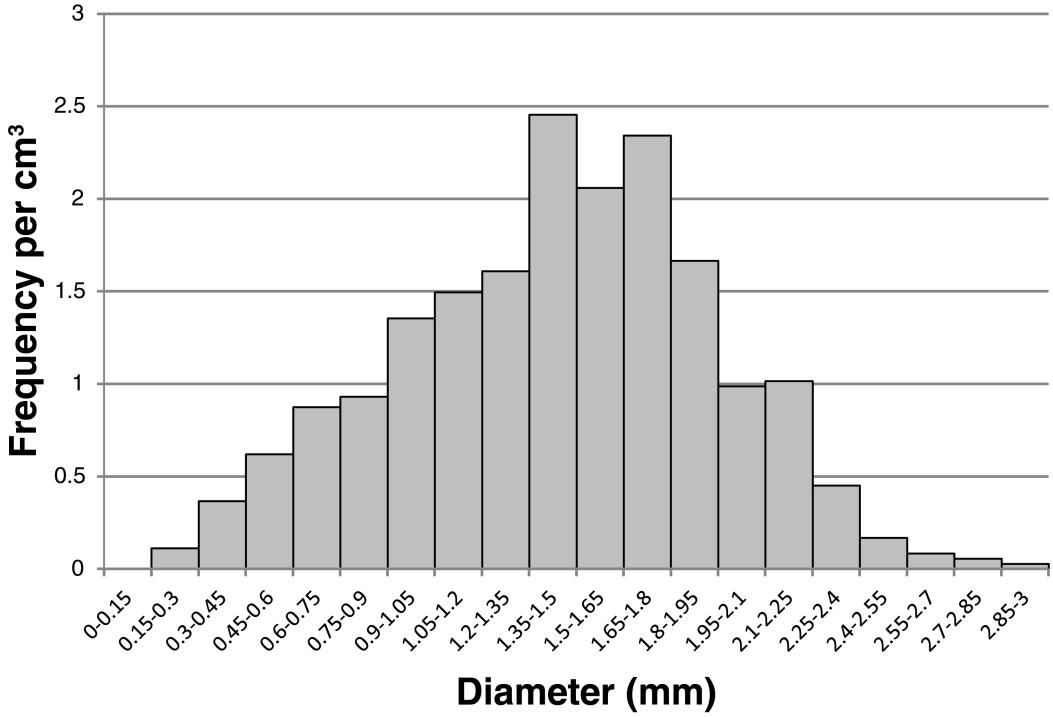

Figure 7. Garnet crystal-size distribution in sample 15RAYJR246A.

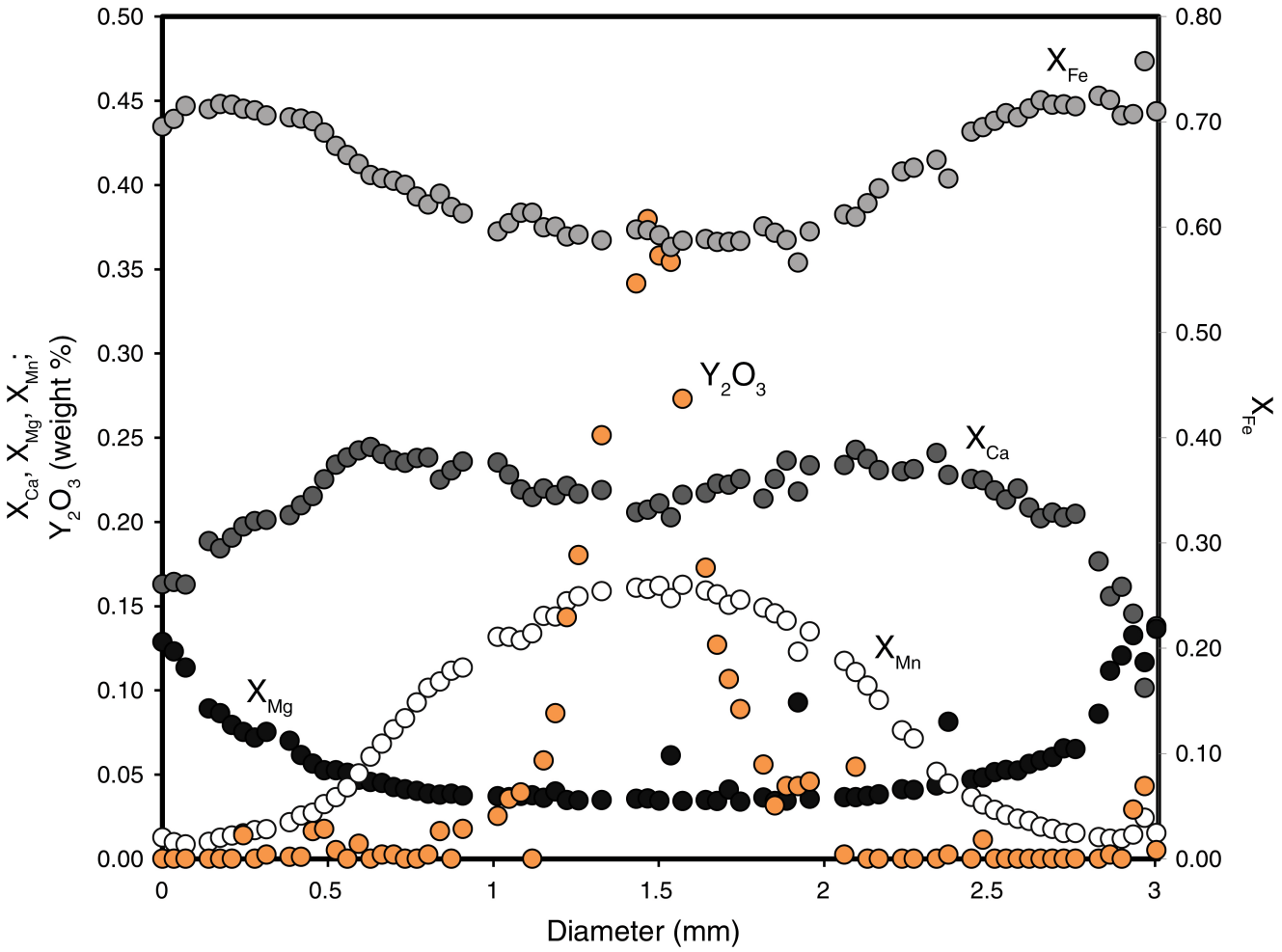

Figure 8. Compositional profile across the geometric centre of the largest garnet crystal identified in sample 15RAYJR246A.

conditions, as can be seen in the stability field of the garnet-bearing assemblages in sample 00RAY231A, which is significantly larger due to a higher bulk MnO concentration (0.28 weight % MnO) relative to other samples (0.10 weight % MnO). Regardless of the different topologies illustrated in the diagrams, the mineral assemblages observed in each of the samples (dark grey fields in Fig. 10) are predicted to be stable at similar conditions, above 550°C and between 6 and 8 kbar. The absence of partial melting sets an upper limit of approximately 700°C for the peak temperature. Garnet isopleths for sample 15RAYJR246A are calculated in Figure 11. With temperature increases, pyrope and almandine contents increase and grossular content decreases. The spessartine content is higher near the garnet-in line, and decreases further away, following an inverse pattern to the volume per cent. The end-member concentrations measured for the core of the largest garnet crystal are shown as red lines and intersect within a precise location close to the garnet-in line.

Metamorphic P-T-t path of garnet crystallization

According to forward modelling of garnet growth and the distribution of garnet isopleths (Fig. 11), garnet growth is inferred to have started at conditions of approximately 510°C and 3.75 kbar and finished at peak P-T conditions of approximately 6.8 kbar and 667°C for sample 15RAYJR246A (Fig. 12; Table 4). Garnet grew over a duration of 27 Ma. The exact heating rate experienced by the sample cannot be determined, but the intracrystalline-diffusion simulations conducted in our study suggest that the rock was subjected to temperatures above 600°C for more than 20 Ma. Figure 13 represents a modelled garnet compositional zoning that fits the observed zoning best for the P-T path suggested in Figure 12, considering different heating scenarios. The model represented by the red line reflects a heating rate of 20°C/Ma until the sample reached 600°C,

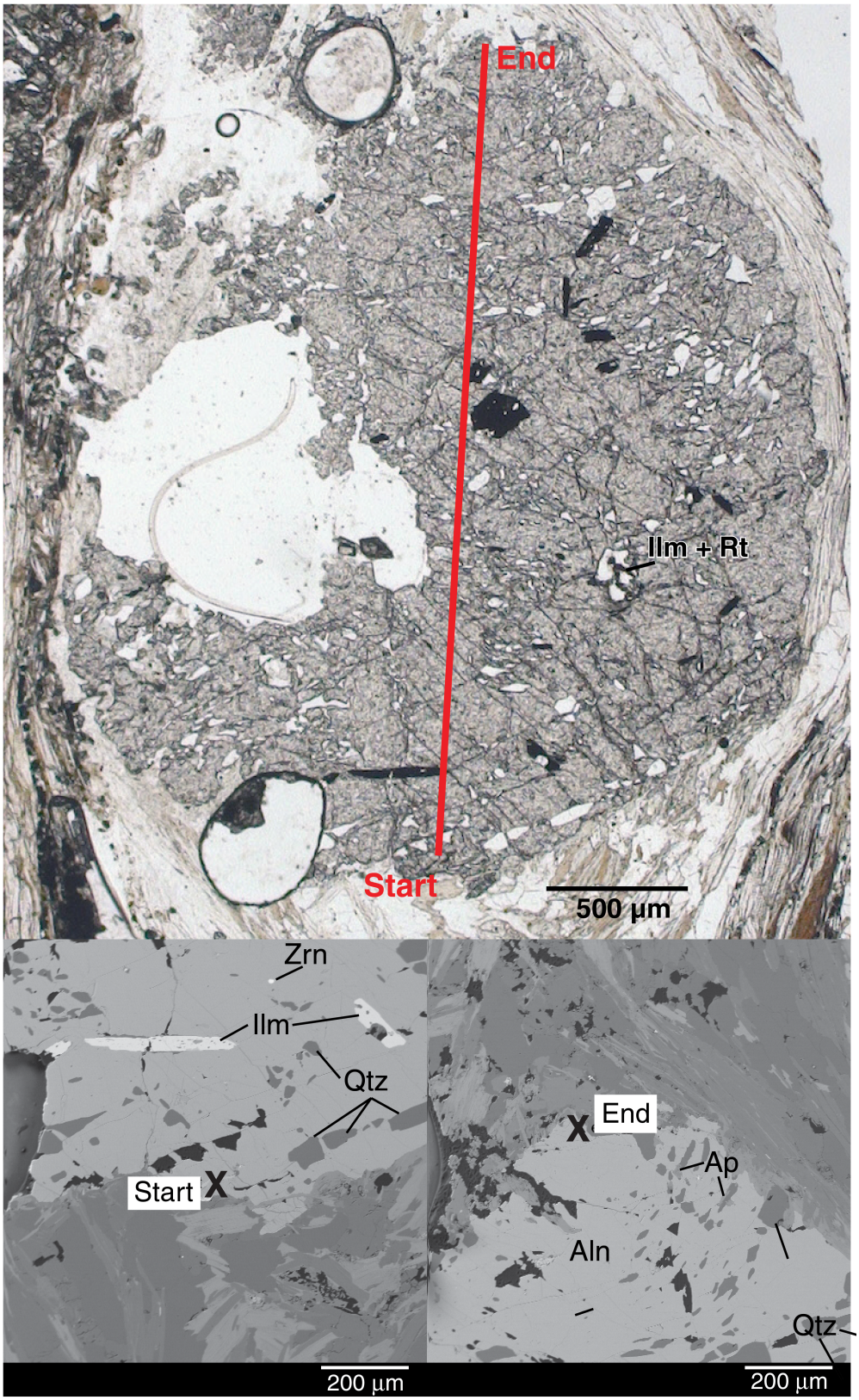

Figure 9. Electron-microprobe transect across the centre of the largest garnet crystal in sample 15RAYJR246A. Inclusions observed include quartz, ilmenite, rutile, apatite, zircon, and allanite. Mineral abbreviations *from* Siivola and Schmid (2007).

Table 3. Garnet core and rim composition, in weight per cent, of the largest garnet crystal in sample 15RAYJR246A, measured through electron-microprobe analysis.

	SiO_2	CaO	Y_2O_3	FeO	Al_2O_3	TiO_2	MnO	MgO	Total
Garnet - core	37.16	7.20	0.38	26.58	20.94	0.09	7.04	0.89	100.26
Garnet - rim	37.29	4.81	0.01	32.66	20.94	0.04	0.68	3.42	99.83

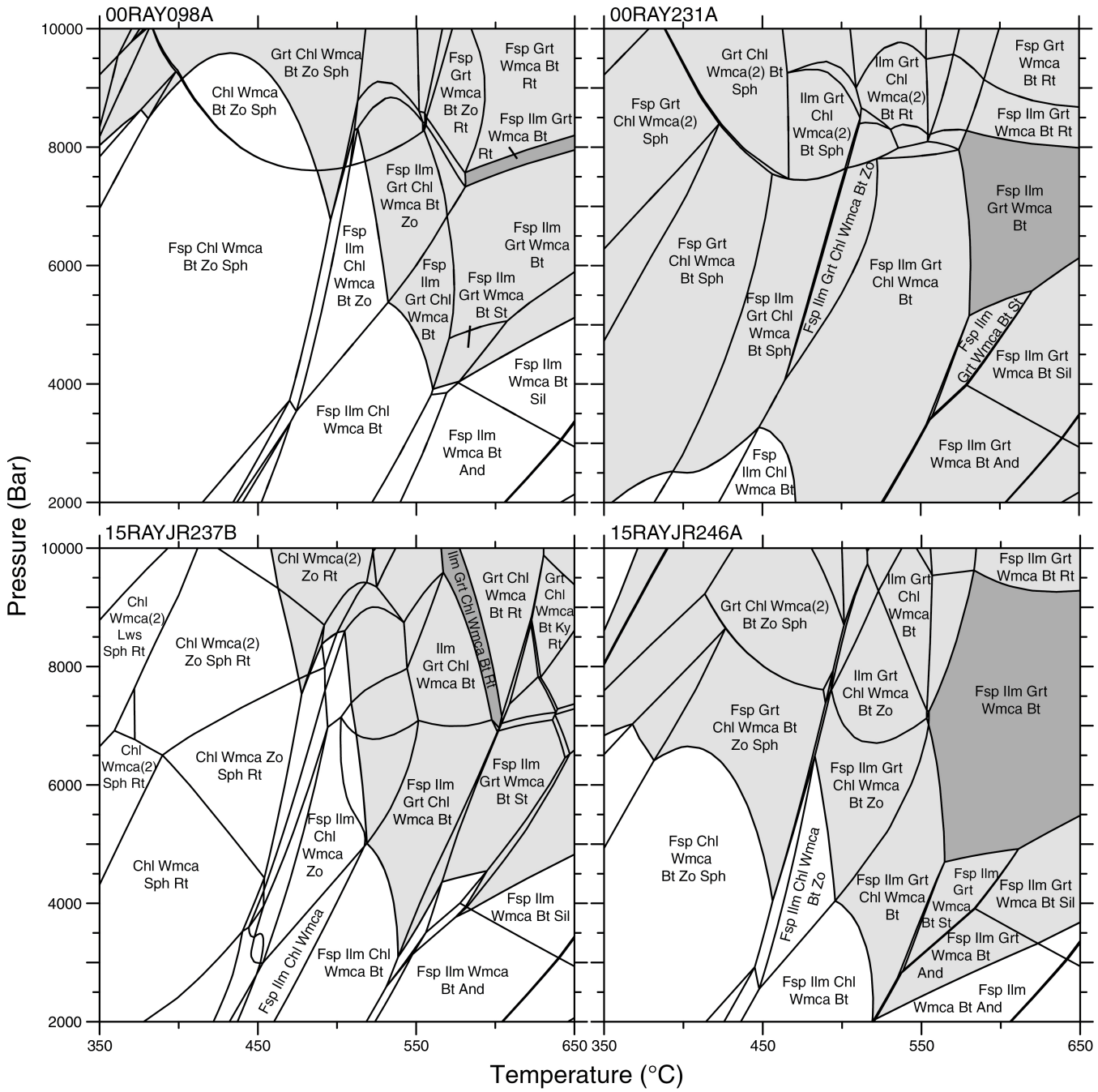

Figure 10. Phase-equilibrium diagrams for samples 00RAY098A, 00RAY231A, 15RAYJR237B, and 15RAYJR246A. The light grey fields represent the predicted P-T conditions of garnet-bearing assemblages, and the dark grey fields reflect the P-T conditions of the assemblages observed in the rocks. Quartz and H_2O are in excess. Wmca = white mica. Other mineral abbreviations *from* Siivola and Schmid (2007).

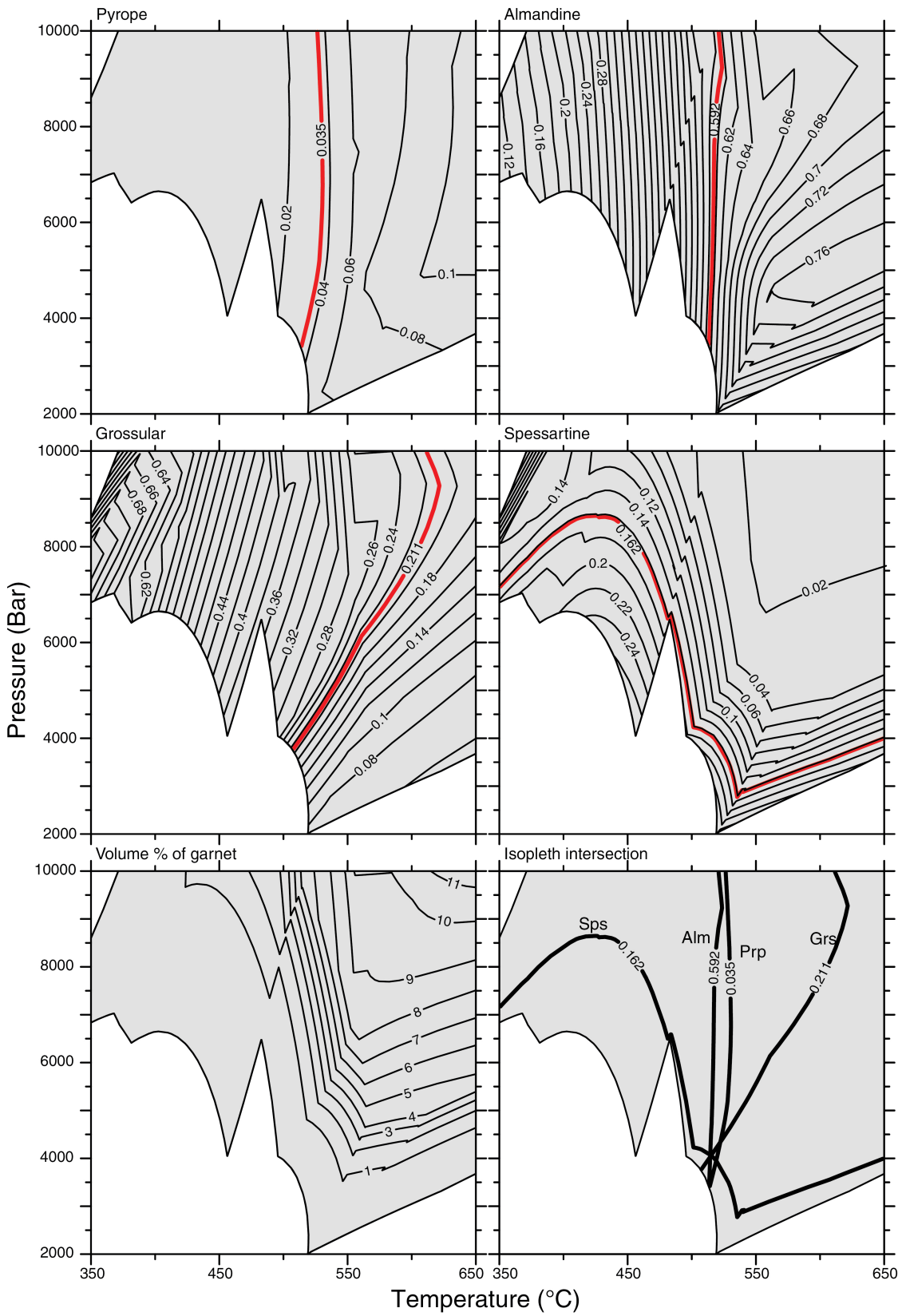

Figure 11. Isopleth diagrams and volume per cent distributions for garnet in sample 15RAYJR246A. Red lines correspond to the chemistry of the core of the largest garnet crystal.

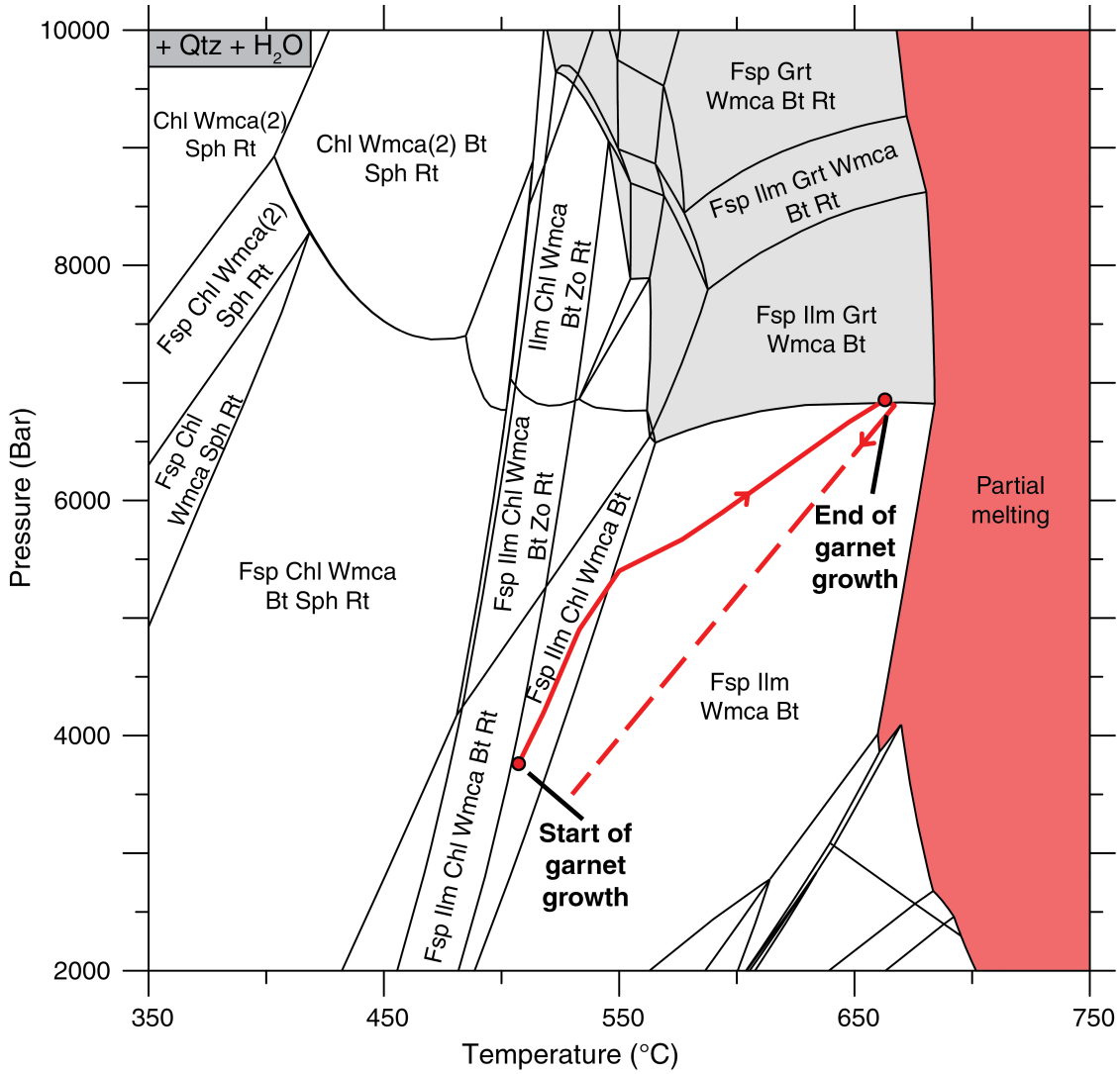

Figure 12. Phase-equilibrium diagram of sample 15RAYJR246A after garnet crystallization finished, with suggested P-T path of garnet growth. Wmca = white mica. Other mineral abbreviations *from* Siivola and Schmid (2007).

followed by a heating rate of 0.85°C/Ma from 650°C to 667°C, keeping the sample at temperatures between 650 and 667°C for 20 Ma (Table 4). The model also predicts the stable mineral assemblage along the path as garnet grows, and only detects a change in the assemblage near the end of the garnet growth, where chlorite leaves the stable assemblage. Figure 12 displays the phase-equilibrium assemblage diagram for the fractionated chemistry of the rock after garnet crystallization. The mineral-assemblage fields differ from the nonfractionated chemistry (Fig. 10), including the garnet field, which moved to significantly higher P-T conditions.

DISCUSSION

Conditions and timing of garnet crystallization

Compositional zoning is commonly observed in metamorphic garnet and can be used to reconstruct P-T-t history (Carlson, 2006; Gaidies et al., 2015; Staples et al., 2014). The largest garnet crystal is assumed to be the first garnet to have started to crystallize; therefore we suggest that its core chemistry best represents the metamorphic conditions present at the transition from a non–garnet-bearing to a garnet-bearing mineral assemblage. With the use of XR-µCT, the central cross-section of the largest garnet crystal can be analyzed, increasing the precision and accuracy of the estimated conditions during the initial growth of garnet.

Table 4. Points along the P-T path and associated heating rates, determined from garnet-crystallization modelling for sample 15RAYJR246A.

Temperature (°C)	Pressure (bar)	Time (Ma)	Heating/cooling rate (°C/Ma)
507	3750	0	20
518	4200	0.55	20
533	4900	1.3	20
550	5400	2.15	20
580	5700	3.65	20
650	6700	7.15	20
667	6800	27.15	0.85
530	3500	28.52	100

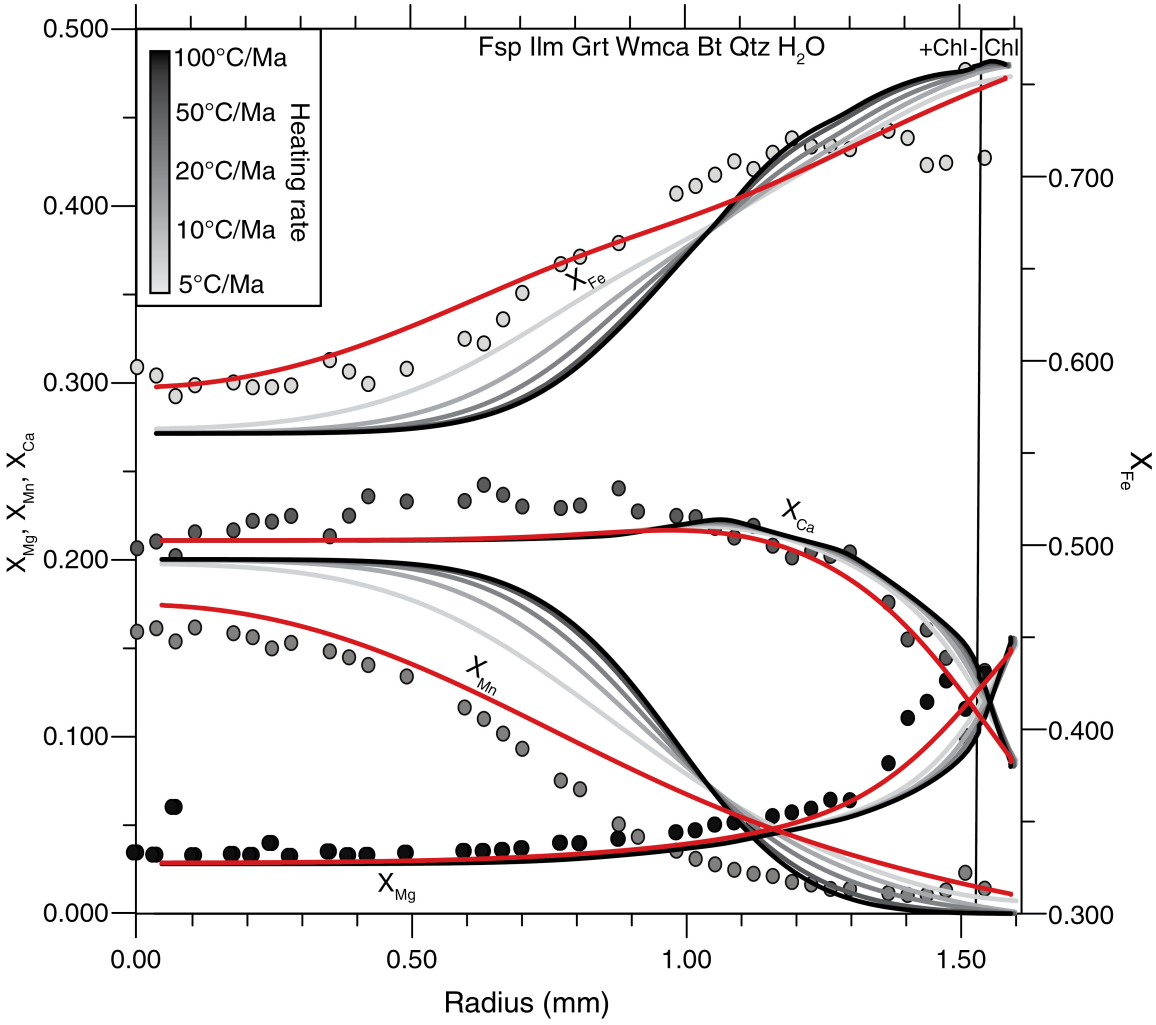

Figure 13. Observed compositional zoning of the largest garnet in sample 15RAYJR246A (symbols) and its predicted garnet chemistry for different heating rates (lines) along the P-T path given in Figure 12. The red lines correspond to the path with the best-fitting heating rate (Table 4). Wmca = white mica. Other mineral abbreviations *from* Siivola and Schmid (2007).

Presence of zoning in the garnet profiles (Fig. 8) indicates that the system is not under complete chemical equilibrium. Thus bulk-rock–composition equilibrium modelling may not produce accurate estimates of the P-T path. The garnet-crystallization modelling performed in this study considers continuous fractionation of elements into garnet and provides better-constrained P-T path information. Phase-equilibrium modelling using the whole-rock chemistry yields a large field of possible peak conditions ranging over 150°C and 4.5 kbar for sample 15RAYJR246A. Garnet-crystallization modelling is significantly more accurate and indicates specific peak conditions of 6.8 kbar and between 667 and 680°C. Further increases in peak metamorphic conditions would yield a larger garnet crystal size than what is observed, with a different garnet-rim composition. Peak temperature can be increased up to 680°C as long as the P-T path remains out of the garnet-bearing stability field. Further increases would result in partial melting, which is not observed in the sample. Increases in peak temperature would increase the diffusion rate, reducing the time required for the sample components to diffuse to the observed levels.

Sample 15RAYJR246A was selected for garnet-crystallization modelling because it is representative of the mineral assemblages and bulk-rock compositions of the samples in this study and it contains garnet crystals with comparatively little evidence of resorption. Different heating rates result in slight variations in the garnet composition. The slower the heating rate, the more time there is for diffusion to occur within garnet. Because Mn and Fe diffuse at a faster rate than Mg and Ca (Chakraborty and Ganguly, 1992), they may be better suited to estimate the amount of diffusion that occurred. Intracrystalline diffusion at a heating rate of 5°C/Ma is not significant enough to match the Mn and Fe contents observed at the core of the garnet. Therefore, a more complex scenario is proposed to increase the influence of diffusion on garnet chemistry, with an initial heating rate of 20°C/Ma, taking 7 Ma to reach conditions of 650°C and 6.7 kbar, followed by a heating rate of 0.85°C/Ma for 20 Ma until peak conditions of 667°C and 6.8 kbar (Table 4). Cooling is modelled to have been exceedingly fast, with a rate of 100°C/Ma. The best-fit model estimates garnet crystallization over 27 Ma. In our simulations, garnet initially grew together with plagioclase, ilmenite, chlorite, white mica, biotite, and quartz. Textural evidence suggests that low-grade rutile was present at low P-T conditions as the main Ti-bearing phase, rather than the predicted sphene in Figure 10. Ilmenite started replacing rutile prior to garnet growth. At a later stage, chlorite left the stable assemblage and was partially consumed by garnet. The continuous chlorite-out reaction initially favoured the transfer of Fe from chlorite to garnet, causing chlorite to become richer in Mg as it was consumed (Inui and Toriumi, 2004). This caused the zoned garnet to experience a steep increase of X_{Fe} at the start of the reaction, followed by a shallower slope of its compositional gradient toward the end of the reaction. According to Inui and Toriumi (2004), the opposite trend is expected for X_{Mg}. The shallow slope of X_{Fe} and sharp increase in X_{Mg} observed at a distance of 1.45 to 1.6 mm from the centre of the modelled garnet profile (Fig. 13) result from the chlorite-out reaction. Similar trends are observed in garnet at a distance of 1.3 to 1.45 mm from the core. This offset of 0.15 mm suggests that the chlorite-out reaction is projected to occur at higher temperatures in the model than what is observed.

Fractionation of elements into garnet during its growth must be considered, as it influences the chemistry of the rocks, which affects the stable mineral-assemblage field. Figure 12 shows the stable mineral assemblages at the end of garnet growth over a range of P-T conditions. Comparison to the stable mineral assemblage without fractionation of garnet (Fig. 10) indicates significant differences, including the noticeable reduction in size of the garnet-stable field and elimination of the staurolite-stable field. These differences highlight the problem of using conventional, nonfractionated phase equilibrium for P-T-t path construction. For example, constructing a P-T-t path that avoids the staurolite field observed in Figure 10 is not necessary, as fractionation of garnet causes a change to a bulk composition that will not crystallize staurolite (Fig. 12). The projected path can therefore cross the staurolite field in Figure 10 without crystallizing staurolite. This results in a different path than what would be obtained if fractionation of garnet chemistry were not considered.

In the absence of metamorphic age constraints, it is difficult to relate the estimated P-T-t path to previous geochronological work. The peak P-T conditions obtained suggest that the sample could have been subjected to either the Permo-Triassic or the Jurassic metamorphic events described by Berman et al. (2007). The pressure estimate is lower than both previously calculated peak pressures, of 9 kbar during the Permo-Triassic and 7.8 kbar during the Jurassic (Berman et al., 2007). Although this pressure difference could be easily accommodated by the distance between samples (>50 km), important variations are also likely, based on the incorporation of garnet zonation and fractionation into P-T modelling. The first metamorphic episode during the Carboniferous could also have impacted these samples, but it would have been overprinted by higher metamorphic conditions.

CONCLUSIONS

The research herein suggests that rocks from the Snowcap assemblage in the Stewart River area have been exposed to at least three deformation events and regional amphibolite-grade metamorphism. The metamorphic episode is syn- to post-tectonic relative to S_{M-1}. The third deformation episode started at the end of garnet growth. Textural evidence suggests a second metamorphic episode further southeast. Garnet-crystallization simulations conducted in this study indicate a metamorphic P-T-t path with peak conditions of 6.8 kbar and 670°C, and a variable heating rate of 20°C/Ma up to 650°C

and 0.85°C/Ma up to 670°C. The observed peak conditions are approximately 1 kbar lower and 75°C higher than the early Jurassic metamorphic peak conditions estimated by Berman et al. (2007), and approximately 2 kbar lower and 70°C higher than the Permian metamorphic peak conditions estimated in the same study. The late Jurassic peak pressure conditions of approximately 7.5 kbar obtained by Staples et al. (2014) in the Yukon-Tanana terrane in the Finlayson Lake district are similar to those obtained in this study, whereas their peak temperature conditions of approximately 600°C are significantly lower. The modelling results presented in this study are therefore similar to conditions previously calculated for the Jurassic event, with the difference in peak pressure being within error of the thermodynamic database, but with peak temperature being significantly higher than previously obtained. The results herein account for garnet compositional zoning, intracrystalline diffusion, and chemical fractionation associated with garnet growth, which are highly sensitive to metamorphic P-T-t changes. Hence, they provide additional and possibly more constrained P-T-t path estimates compared to those obtained in earlier studies, which did not consider intracrystalline diffusion or were based on metamorphic phase equilibria between garnet and the rock matrix.

AKNOWLEDGMENTS

We would like to thank P. Jones (Carleton University) for the electron-microprobe assistance, and D. Regis (Geological Survey of Canada) for the thorough review of this article. This research was supported by the Geological Survey of Canada's Geo-mapping for Energy and Minerals program (GEM-2 – Cordillera).

REFERENCES

Beranek, L.P. and Mortensen, J.K., 2011. The timing and provenance record of the Late Permian Klondike orogeny in northwestern Canada and arc-continent collision along western North America; Tectonics, v. 30, cit. no. TC5017. https://doi.org/10.1029/2010TC002849

Beranek, L.P., Mortensen, J.K., Orchard, M.J., and Ullrich, T., 2010. Provenance of North American Triassic strata from west-central and southeastern Yukon: correlations with coeval strata in the Western Canada Sedimentary Basin and Canadian Arctic Islands; Canadian Journal of Earth Sciences, v. 47, no. 1, p. 53–73. https://doi.org/10.1139/E09-065

Berman, R.G., Ryan, J.J., Gordey, S.P., and Villeneuve, M., 2007. Permian to Cretaceous polymetamorphic evolution of the Stewart River region, Yukon-Tanana terrane, Yukon, Canada: P-T evolution linked with in situ SHRIMP monazite geochronology; Journal of Metamorphic Geology, v. 25, no. 7, p. 803–827. https://doi.org/10.1111/j.1525-1314.2007.00729.x

Caddick, M.J., Konopasek, J., and Thompson, A.B., 2010. Preservation of garnet growth zoning and the duration of prograde metamorphism; Journal of Petrology, v. 51, no. 11, p. 2327–2347. https://doi.org/10.1093/petrology/egq059

Canil, D., Johnston, S.T., Evers, K., Shellnutt, J.G., and Creaser, R.A., 2003. Mantle exhumation in an early Paleozoic passive margin, northern Cordillera, Yukon; The Journal of Geology, v. 111, no. 3, p. 313–327. https://doi.org/10.1086/373971

Carlson, W.D., 2006. Rates of Fe, Mg, Mn, and Ca diffusion in garnet; The American Mineralogist, v. 91, no. 1, p. 1–11. https://doi.org/10.2138/am.2006.2043

Chakraborty, S. and Ganguly, J., 1992. Cation diffusion in aluminosilicate garnets – experimental determination in spessartine-almandine diffusion couples, evaluation of effective binary diffusion-coefficients, and applications; Contributions to Mineralogy and Petrology, v. 111, no. 1, p. 74–86. https://doi.org/10.1007/BF00296579

Clark, A.D., Gibson, H.D., Staples, R.D., Israel, S., and Crowley, J.L., 2016. Timing of mid-crustal tectono-metamorphism in Yukon-Tanana terrane at Aishihik Lake, southwest Yukon; Geological Association of Canada-Mineralogical Association of Canada, Abstracts, v. 39, p. 12-13.

Colpron, M. and Nelson, J.L., 2011. A digital atlas of terranes for the Northern Cordillera; Yukon Geological Survey. <www.geology.gov.yk.ca> [accessed December 3, 2016]

Colpron, M. and Ryan, J.J., 2009. Bedrock geology of southwest McQuesten (NTS 115P) and part of northern Carmacks (NTS 115I) map area; *in* Yukon Exploration and Geology 2009, (ed.) K.E. MacFarlane, L.H. Weston and L.R. Blackburn, Yukon Geological Survey, p. 159–184.

Cox, R., Lowe, D.R., and Cullers, R.L., 1995. The influence of sediment recycling and basement composition on evolution of mudrock chemistry in the southwestern United States; Geochimica et Cosmochimica Acta, v. 59, no. 14, p. 2919–2940. https://doi.org/10.1016/0016-7037(95)00185-9

de Capitani, C. and Petrakakis, K., 2010. The computation of equilibrium assemblage diagrams with Theriak/Domino software; The American Mineralogist, v. 95, no. 7, p. 1006–1016. https://doi.org/10.2138/am.2010.3354

Dickinson, W.R., 2004. Evolution of the North American Cordillera; Annual Review of Earth and Planetary Sciences, v. 32, p. 13–45. https://doi.org/10.1146/annurev.earth.32.101802.120257

Dusel-Bacon, C., Hansen, V.L., and Scala, J.A., 1995. High-pressure amphibolite facies dynamic metamorphism and the Mesozoic tectonic evolution of an ancient continental margin, east-central Alaska; Journal of Metamorphic Geology, v. 13, no. 1, p. 9–24. https://doi.org/10.1111/j.1525-1314.1995.tb00202.x

Ferry, J.M. and Spear, F.S., 1978. Experimental calibration of the partitioning of Fe and Mg between biotite and garnet; Contributions to Mineralogy and Petrology, v. 66, no. 2, p. 113–117. https://doi.org/10.1007/BF00372150

Florence, F.P. and Spear, F.S., 1991. Effects of diffusional modification of garnet growth zoning on P-T path calculations; Contributions to Mineralogy and Petrology, v. 107, no. 4, p. 487–500. https://doi.org/10.1007/BF00310683

Gaidies, F., de Capitani, C., and Abart, R., 2008. THERIA_G: a software program to numerically model prograde garnet growth; Contributions to Mineralogy and Petrology, v. 155, no. 5, p. 657–671. https://doi.org/10.1007/s00410-007-0263-z

Gaidies, F., Petley-Ragan, A., Chakraborty, S., Dasgupta, S., and Jones, P., 2015. Constraining the conditions of Barrovian metamorphism in Sikkim, India: P-T-t paths of garnet crystallization in the Lesser Himalayan Belt; Journal of Metamorphic Geology, v. 33, no. 1, p. 23–44. https://doi.org/10.1111/jmg.12108

Garcia, D., Coelho, J., and Perrin, M., 1991. Fractionation between $Ti0_2$ and Zr as a measure of sorting within shale and sandstone series (northern Portugal); European Journal of Mineralogy, v. 3, no. 2, p. 401–414. https://doi.org/10.1127/ejm/3/2/0401

Ghent, E., 1975. Temperature, pressure, and mixed-volatile equilibria attending metamorphism of staurolite-kyanite-bearing assemblages, Esplanade Range, British Columbia; Geological Society of America Bulletin, v. 86, no. 12, p. 1654–1660. https://doi.org/10.1130/0016-7606(1975)86<1654:TPAMEA>2.0.CO;2

Gordey, S.P. and Ryan, J.J., 2005. Geology, Stewart River area (115 N, 115-O and part of 115J), Yukon Territory; Geological Survey of Canada, Open File 4970, scale 1:250 000. https://doi.org/10.4095/221149

Gordey, S.P., Williams, S.P., Cocking, R.B., and Ryan, J.J., 2006. Digital geology, Stewart River area, Yukon; Geological Survey of Canada, Open File 5122, 1 DVD-ROM. https://doi.org/10.4095/221967

Herron, M.M., 1988. Geochemical classification of terrigenous sands and shales from core or log data; Journal of Sedimentary Petrology, v. 58, no. 5, p. 820–829.

Holland, T.J.B. and Powell, R., 1998. An internally consistent thermodynamic data set for phases of petrological interest; Journal of Metamorphic Geology, v. 16, no. 3, p. 309–343. https://doi.org/10.1111/j.1525-1314.1998.00140.x

Inui, M. and Toriumi, M., 2004. A theoretical study on the formation of growth zoning in garnet consuming chlorite; Journal of Petrology, v. 45, no. 7, p. 1369–1392. https://doi.org/10.1093/petrology/egh016

Johnston, S.T., Canil, D., and Heaman, L.H., 2007. Permian exhumation of the Buffalo Pitts orogenic peridotite massif, northern Cordillera, Yukon; Canadian Journal of Earth Sciences, v. 44, no. 3, p. 275–286. https://doi.org/10.1139/e06-078

Joyce, N.L., Ryan, J.J., Colpron, M., Hart, C.J.R., and Murphy, D.C., 2015. A compilation of 40Ar/39Ar age determinations for igneous and metamorphic rocks, and mineral occurrences from central and southeast Yukon; Geological Survey of Canada, Open File 7924, 1. zip file. https://doi.org/10.4095/297446.

Logan, J.M. and Mihalynuk, M.G., 2014. Tectonic controls on early Mesozoic paired alkaline porphyry deposit belts (Cu-Au ± Ag-Pt-Pd-Mo) within the Canadian Cordillera; Economic Geology and the Bulletin of the Society of Economic Geologists, v. 109, p. 827–858. https://doi.org/10.2113/econgeo.109.4.827

Monger, J.W.H. and Price, R.A., 2002. The Canadian Cordillera: Geology and tectonic evolution; Canadian Society of Exploration Geophysicists Recorder, v. 27, p. 17–36.

Nelson, J.L., Colpron, M., and Israel, S., 2013. The Cordillera of British Columbia, Yukon, and Alaska: Tectonics and metallogeny; *in* Tectonics, metallogeny and discovery: the North American Cordillera and similar accretionary settings, (ed.) M. Colpron, T. Bissig, B.G. Rusk, and J.F.H. Thompson; Society of Economic Geologists, Special Publication 17, p. 53–103.

Norrish, K. and Hutton, J.T., 1969. An accurate X-ray spectrographic method for the analysis of a wide range of geological samples; Geochimica et Cosmochimica Acta, v. 33, no. 4, p. 431–453. https://doi.org/10.1016/0016-7037(69)90126-4

Piercey, S.J. and Colpron, M., 2009. Composition and provenance of the Snowcap assemblage, basement to the Yukon-Tanana terrane, northern Cordillera: Implications for Cordilleran crustal growth; Geosphere, v. 5, no. 5, p. 439–464. https://doi.org/10.1130/GES00505.S3

Piercey, S.J., Nelson, J.L., Colpron, M., Dusel-Bacon, C., Simard, R.-L., and Roots, C.F., 2006. Paleozoic magmatism and crustal recycling along the ancient Pacific margin of North America, northern Cordillera; *in* Paleozoic evolution and metallogeny of pericratonic terranes at the ancient Pacific margin of North America, Canadian and Alaskan Cordillera, (ed.) M. Colpron and J.L. Nelson; Geological Association of Canada, Special Paper 45, p. 281–322.

Roser, B.P. and Korsch, R.J., 1986. Determination of tectonic setting of sandstone-mudstone suites using SiO_2 content and K_2O-Na_2O ratio; The Journal of Geology, v. 94, no. 5, p. 635–650. https://doi.org/10.1086/629071

Ryan, J.J., Zagorevski, Z., Roots, C.F., and Joyce, N., 2014. Paleozoic tectonostratigraphy of the northern Stevenson Ridge area, Yukon; Geological Survey of Canada, Current Research 2014–4, 13 p. https://doi.org/10.4095/293924

Siivola, J. and Schmid, R., 2007. Recommendations by the IUGS Subcommission on the systematics of metamorphic rocks: List of mineral abbreviations: Web version 01.02.07; IUGS Commission on the Systematics in Petrology. <http://www.bgs.ac.uk/scmr/docs/papers/paper_12.pdf>

Spear, F.S., Kohn, M.J., Florence, F.P., and Menard, T., 1991. A model for garnet and plagioclase growth in pelitic schists: implications for thermobarometry and P-T path determinations; Journal of Metamorphic Geology, v. 8, p. 683–696. https://doi.org/10.1111/j.1525-1314.1990.tb00495.x

Staples, R.D., Gibson, H.D., Berman, R.G., Ryan, J.J., and Colpron, M., 2013. A window into the Early to mid-Cretaceous infrastructure of the Yukon-Tanana terrane recorded in multi-stage garnet of west-central Yukon, Canada; Journal of Metamorphic Geology, v. 31, no. 7, p. 729–753. https://doi.org/10.1111/jmg.12042

Staples, R.D., Murphy, D.C., Gibson, H.D., Colpron, M., Berman, R.G., and Ryan, J.J., 2014. Middle Jurassic to earliest Cretaceous mid-crustal tectono-metamorphism in the northern Canadian Cordillera: Recording foreland-directed migration of an orogenic front; Geological Society of America Bulletin, v. 126, no. 11–12, p. 1511–1530. https://doi.org/10.1130/B31037.1

Staples, R., Gibson, H.D., Colpron, M., and Ryan, J.J., 2016. An orogenic wedge model for diachronous deformation, metamorphism, and exhumation in the hinterland of the northern Canadian Cordillera; Lithosphere, v. 8, no. 2, p. 165–184. https://doi.org/10.1130/L472.1

Symmes, G.H. and Ferry, J.M., 1991. Evidence from mineral assemblages for infiltration of pelitic schists by aqueous fluids during metamorphism; Contributions to Mineralogy and Petrology, v. 108, no. 4, p. 419–438. https://doi.org/10.1007/BF00303447

Thompson, J.B., 1957. The graphical analysis of mineral assemblages in pelitic schists; The American Mineralogist, v. 42, p. 842–858.

Woodsworth, G.J., Anderson, R.G., and Armstrong, R.L., 1991. Plutonic regimes; *in* Geology of the Cordilleran Orogen in Canada, (ed.) H. Gabrielse and C.J. Yorath; Geological Survey of Canada, Geology of Canada, no. 4 (also Geological Society of America, The geology of North America, v. G-2), p. 491–531.

Geological Survey of Canada Project 340552NU62